Mechanics and Mechanical Engineering
Vol. 20, No. 4 (2016) 467–488

Mathematical and Experimental Analysis Tension of Steel in Bi-Polar Coordinates

Mieczysław Jaroniek
Department of Strength of Materials
Lodz University of Technology
Stefanowskiego 1/15, 90–924 Łódź, Poland

Received (10 June 2016)
Revised (5 August 2016)
Accepted (20 November 2016)

A series of experiments was carried out to examine the effects of elastic–plastic deformation on the state of stress and the flow stress mechanism under static tension. The strain distribution determined from the fringe pattern using the Moire method allows one to determine the strain and the crack propagation of not–notched specimens an isotropic and elastic–plastic materials. In the analysis of stress the method of calculating using the bipolar coordinate is proposed. The theoretical model is divided into two elements and the condition of incompressibility is satisfied in each element. The proposed method is compared with the elastic-plastic FEM (ANSYS 12, 14) and it is satisfied approximately. The tensile test is aimed to verify the mathematical model that can be applied in the logarithmic stain in further computations.

Keywords: stress–strain relationship; bi–polar coordinates; moiré method; finite element method.

1. Introduction

The results of experimental investigations are the basic element in formulating of theoretical solutions. However, despite of dynamic development in measuring techniques, an interpretation of test results can be difficult due to a limited spectrum and range of applicability of the apparatus used in tests. It seems that an application of latest calculation methods allows one to determine the boundary states and to failure phases of a structure or an element on the basis of material properties. However, investigation methods are continuously modernised and the results of some research are protected by patents and made public unwillingly in numerous cases, thus such data should be supplemented with additional measurements, e.g., of strains in the failure phase, the determination of crack resistance, etc.

Strength resistance properties of materials are the basic element that enables calculations and formulation of theoretical solutions, however due to their limited

spectrum in case of complex stresses and strains, their explicit interpretation can be impeded. As a classical example of such an approach, one can consider a simple tensile test as the basis for further calculations. The analysis of the failure phase under tension has been presented, for example in [1], [3], [6], [23] and al.

Tension diagrams that characterize the material properties are treated as the fundamental element of numerical computations. Testing machines that has been using currently allow one to describe precisely tensile tests, but their software enables the determination of only some parameters that define the material properties. The application of results of typical strength tests into numerical computations is incurred with errors that follow from the simplifications assumed. A lack of mathematical model, which would describe an actual $\sigma - \varepsilon$ (stress–strain) relationship in the whole range of load, compels designers to use simplified assumptions or to conduct additional recalculations in order to describe the complete tensile behaviour, including the failure phase. The investigations carried out by the author allow one to analyse subsequent tension phases, a failure mode and an occurrence of sliding planes and an actual $\sigma - \varepsilon$ relationship. The analysis of stress and strain states for steel was made on an Instron testing machine. The displacement and strain measurements presented in this study were made with strain gauges, an extensometer and by means of the moiré–fringe technique [7, 14] and all. A detailed analysis of such measurements is founded in the next section of the present study. A description of the stress-strain relationship, which takes into consideration strain hardening, and next necking until the moment of rupture, along with a description of breaking stresses, allows one to build such a mathematical model in the whole range of load, which accounts for the fracture formation and the element failure.

The way the strains are described in bi–polar coordinates, which has been based on the experimental investigations, makes it possible to employ the results in the numerical computations, wherever we are interested in stress states in the failure phase. The real $\sigma - \varepsilon$ (stress–strain) relationship used in calculations (in elastic–plastic materials after strain hardening) comprises a description of strains until the moment of an occurrence of necking, next it describes a stress distribution after the occurrence of necking, and the process of fracture itself is described on the basis of tests of specimens with existing fissures.

The investigations of the fracture process and the analysis of causes of the scratch occurrence are the object of numerous scientific investigations and studies, and the complete range of methods and solutions, which examples are listed at the end of this study, fall beyond the scope of the present study. In this study, some test and calculation methods that can be employed to develop a model of structures, which then can be used in the engineering practice in the whole range of loading and which accounts for element fracture and failure investigations have been presented. The numerical calculation results, and especially the finite element method, are now widely used in structure calculations. For instance, the professional ANSYS software allows for carrying out all kinds of computations. In this program in the range of elastic–plastic strains, the logarithmic stain $\varepsilon_l$is assumed instead of the conventional strain ε, and the value of the Poisson's ratio $\nu_{pl}(\varepsilon)$ is assumed as a constant and equal to 0.5, which agrees approximately with the real state of stresses and strains.

2. Results of tensile tests

The diagrams $F(\Delta l)$ or $\sigma(\varepsilon)$ obtained from the testing machine should be interpreted so that the diagram $\sigma(\varepsilon)$ should correspond to real $\sigma - \varepsilon$ relationships. The characteristic quantities, on the basis of which the $\sigma - \varepsilon$ relationship can be formed, are the forces corresponding to the physical yield point or the proof stress, the maximum force and the strain corresponding to it, and the force acting when the specimen is necked and ruptured. For each of these forces, the cross-sectional dimensions can be measured and the stresses calculated, and then an approximate variability of the function $\sigma(\varepsilon)$ can be calculated. The values obtained in the strength tests and the quantities determined on their basis are depicted in Fig. 1. The plot $\sigma(\varepsilon)$ obtained from the testing machine is a conventional plot, the value of the force divided by a constant value of the cross-section is given on the vertical axis, whereas the elongation related to the initial length, that is to say, the relative strain (also called the conventional strain) is presented on the horizontal axis. Thus, as a matter of fact this diagram is a copy of the F(Δl) plot, in another system of coordinates. The quantities obtained on the basis of the strength tests are as follows:

1. limit of proportionality $\sigma_p = \sigma_{prop}$ and the strain corresponding to it $\varepsilon_p = \varepsilon_{prop}$ and the Young's modulus E,

2. proof stress or physical yield point - R_{02} , R_e ($\sigma_0 = \sigma_{pl}$ and the strain corresponding to it $\varepsilon_0 = \varepsilon_{pl}$),

3. maximum force F_{max} - tensile strength R_m , real stress (σ_{rz}) corresponding to R_m, force corresponding to necking F_{kr} – maximum stress (σ_{max}) corresponding to rupture.

Beside standard results given in typical reports, actual values of stresses corresponding to the tensile strength and the rupture force are given as well.

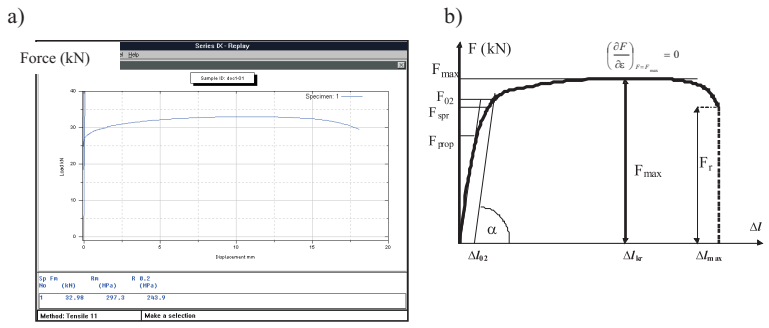

Figure 1 Tension diagrams $F(\Delta l)$ – force–elongation: a) diagram obtained from the Instron testing machine, b) general diagram with characteristic quantities that enable a description of the material properties

Note : the real stresses have been defined as a ratio of the maximum force to the area of the actual cross–section (according to formula 3), on the assumption that we have uniform tension until the maximum tensile force is achieved, e.g.:

$$\sigma_{rz} = \frac{F_{\max}}{b(\varepsilon) \cdot h(\varepsilon)} = \frac{F_{\max}}{b_0 h_0 \cdot (1 - \varepsilon_{kr} \cdot \nu_{pl})^2} = 357.2\, MPa$$

and when this force is exceeded, we can observe a further development of plastic strains and an occurrence of necking, and the maximum stresses have been defined as a ratio of the rupture force to the necked cross–section area A_p:

$$\sigma_{\max} = \frac{F_{kr}}{A_p} = \frac{F_{\max}}{b_{\min} h_{\min}} = 510.6\, MPa$$

2.1. *Description of the displacement measurement method and results of tests and calculations*

Displacements of the specimen surface in the point of an occurrence of necking and fracture just before failure were determined by means of the moiré–fringe technique. Owing to the simplicity of this method and relatively large strains, a shadow method was employed [7, 14]. The measurement principle are shown in Fig. 2. Moiré half–tone screens were located parallel to the specimen surface, then the specimens were illuminated at the angle $\varphi = 30^o \div 40^o$, and the moiré–fringe patterns corresponding to perpendicular displacements that characterise changes in thickness and sliding lines were photographed.

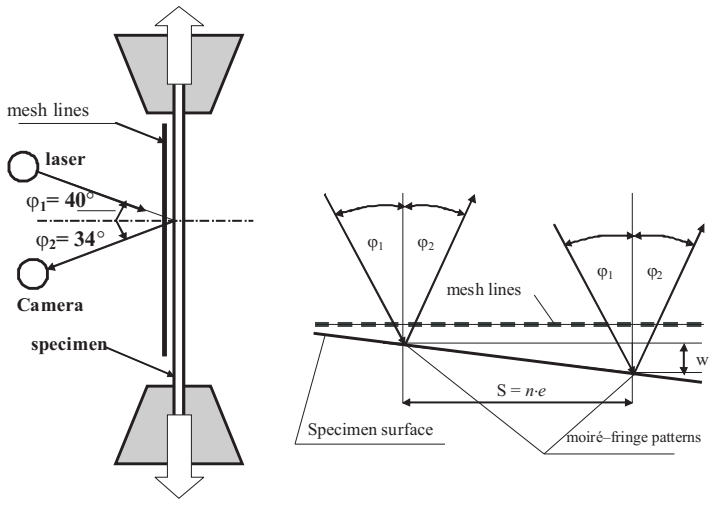

Figure 2 Displacement measurement principle on the specimen surface

Next, the results of tests and calculations were compared for the given values: $e = 1/13$ mm, $\varphi_1 = 40^o$, $\varphi_2 = 34^o$, w $\cong$ 0.051mm. The difference in height corresponding to the distance S between the neighbouring moiré-fringe patterns was calculated according to the formula:

$$w = \frac{e}{tg\varphi_1 + tg\varphi_2} \tag{1}$$

where:

e – mesh pitch (distance between mesh lines per 1 mm),

w – difference in height corresponding to the length S between the subsequent moiré–fringe patterns,

φ_1 – angle of incidence of the parallel light beam,

φ_2 – camera inclination angle,

$w = 0.408$ mm, $2w = 0.816$ mm, $h_s = 0.54 \div 0.66$ mm,

$h_{min} = 1.356 \div 1.476$ mm (1.4 mm).

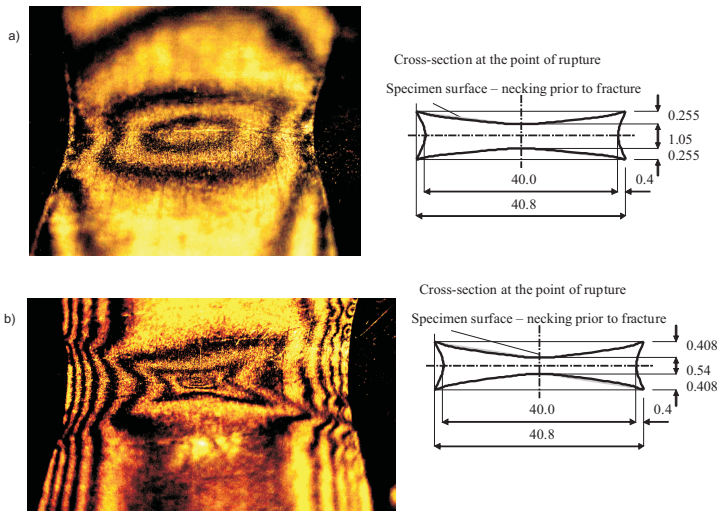

Figure 3 Distribution of the moiré–fringe patterns: a) occurrence of necking, b) prior to rupture on the surface (in the middle of the specimen) and changes in the cross-section at the point of rupture obtained with the moiré–fringe technique

2.2. *Theoretical description of tension – modification of the Ramberg–Osgood curve*

On the basis of physical and geometrical relations for plain stress, strains and stresses can be calculated if we characterize the material by the Ramberg–Osgood curve [3,6,8], [12,13]:

$$\varepsilon_{ij}^{pl} = \frac{3}{2}\alpha\varepsilon_o \left(\frac{\sigma_e}{\sigma_o}\right)^{n-1} \frac{S_{ij}}{\sigma_o} \tag{2}$$

The non–linear relationship $\sigma - \varepsilon$ is usually assumed in the form (assuming for simplicity that $p = 1/n$) [3]:

$$\begin{aligned} &\text{for} \quad \varepsilon \leq \varepsilon_0 \quad \sigma = \left(\frac{\sigma_0}{\varepsilon_0}\right)\varepsilon \\ &\text{for} \quad \varepsilon > \varepsilon_0 \qquad \varepsilon = \alpha\,\varepsilon_0 \left(\frac{\sigma}{\sigma_0}\right)^{\frac{1}{p}} \quad \Rightarrow \quad \sigma = \frac{1}{\alpha}\sigma_0 \left(\frac{\varepsilon}{\varepsilon_0}\right)^{p} \end{aligned} \tag{3}$$

According to the author's point of view, an effect of transverse strains should be considered under large strains. To simplify the issue (for large plastic strains or elastic–plastic strains), one can assume that the dimensions of the rectangular cross–section ($b_0 \times h_0$) change according to the following relationship:

$$b(\varepsilon_x) = b_0\,(1 - \nu_{pl}\varepsilon_y)\,, \quad h(\varepsilon_z) = h_0\,(1 - \nu_{pl}\varepsilon_y)\,, \quad \varepsilon_x = \varepsilon_z = -\nu_{pl}\varepsilon_y \tag{4}$$

and:
for $\varepsilon > \varepsilon_0$, the equivalent Poisson's ratio for elastic–plastic materials, according to [3, 8, 9], takes the form: $\nu_{pl} = \frac{1}{2} - \frac{1-2\nu_0}{2E_0}\frac{\sigma}{\varepsilon}$

The Poisson's ratio ν_{pl} is a function of strain and varies during the process of deformation $\nu_{pl}(\varepsilon)$. After the substitution of:

$$\alpha = 1 \text{ and } E_0 = \frac{\sigma_0}{\varepsilon_0} \qquad \sigma = \sigma_0 \left(\frac{\varepsilon}{\varepsilon_0}\right)^{p} \tag{5}$$

$$\nu_{pl} = \frac{1}{2} - \frac{1-2\nu_0}{2}\left(\frac{\varepsilon}{\varepsilon_0}\right)^{p-1} \tag{6}$$

where: $\nu_0 \cong 0.3$.

In individual phases of tension, we can determine approximately strains on the basis of tests, having the initial dimensions and the tension diagram in form (5).

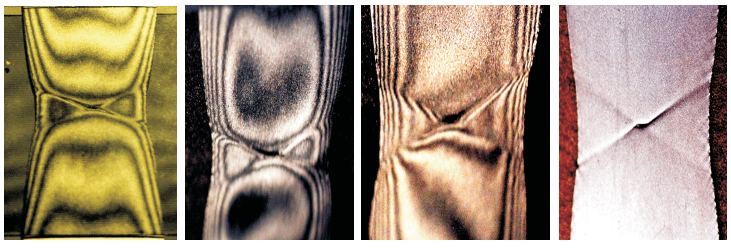

Figure 4 An examples of the distributions of the moiré-fringe patterns corresponding to an occurrence of the plastic strain zone, then fractures in the middle, and, consequently, the failure of the specimen

2.3. *Conventional and logarithmic strain*

Other methods of the description of the relationship $F(\varepsilon)$ have been presented in [2, 4, 6, 9, 24]. Starting from the logarithmic strains ε_t proposed by Ludwik [11], the conventional strain ε is related to the logarithmic one ε_t by the following relationship: $\varepsilon_t = \ln(1+\varepsilon)$. An elementary increment of the conventional strain $(d\varepsilon)$ expresses a change in the length with respect to the initial length l_0, whereas an increment of the logarithmic strain $d\varepsilon_t$ expresses a change of the length with respect to the instantaneous length l. These strains are written as follows:

$$d\varepsilon = \frac{dl}{l_0} \Rightarrow \varepsilon = \frac{l - l_0}{l_0} \qquad d\varepsilon_t = \frac{dl}{l} \rightarrow \varepsilon_t = \ln\frac{l}{l_0} \tag{7}$$

where: $l = l_0(1+\varepsilon)$ and thus we obtain:

$$\varepsilon_t = \ln(1+\varepsilon) \tag{8}$$

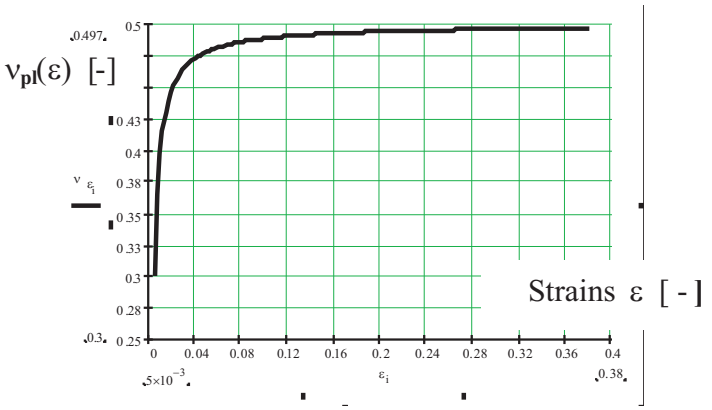

Figure 5 Changes in the Poisson's ratio $\nu_{pl}(\varepsilon)$ according to formula (6) as a function of strain $\nu(\varepsilon)$ for $\nu_0 = 0.3$ and $p = 0.1$

Taking into account the above–mentioned assumptions, we can calculate the value of the tensile force from the formula:

$$F = \sigma(\varepsilon)\, A(\varepsilon) \tag{9}$$

where the stresses $\sigma(\varepsilon)$ and the cross–section $A(\varepsilon)$ are functions of strains. Starting with the condition of instability in tension, that is to say, for $F = F_{max}$, $\partial F/\partial\varepsilon_1 = 0$ (on assumption that ε_1 corresponds to the tension direction, and ε_2 and ε_3 are main strains perpendicular to ε_1), the following has been obtained:

$$\frac{dF}{d\varepsilon_1} = \frac{d\sigma}{d\varepsilon_1}A + \sigma\frac{dA}{d\varepsilon_1} = 0 \quad \text{where: } A = A_0(1+\varepsilon_2)(1+\varepsilon_3) = A_0 e^{\varepsilon_{t2}} e^{\varepsilon_{t3}} \tag{10}$$

Having taken into account the incompressibility condition that is defined by the logarithmic dilatational strain:

$$\Delta V = \ln(1+\Delta V) = \varepsilon_{t1} + \varepsilon_{t2} + \varepsilon_{t3} \qquad \Delta V = 0$$
$$\varepsilon_{t1} + \varepsilon_{t2} + \varepsilon_{t3} = 0 \rightarrow \varepsilon_{t2} + \varepsilon_{t3} = -\varepsilon_{t1} \text{ and } A_1 = A_0 e^{\varepsilon_{t1}}$$

we obtain:

$$\frac{dA}{d\varepsilon_{t1}} = -A_0 e^{\varepsilon_{t1}} = -A$$

Having substituted the above-mentioned equation into (10) and having divided it by A, we get the condition of instability in tension as follows:

$$\frac{d\sigma}{d\varepsilon_1} = \sigma_1 \tag{11}$$

The conventional dilatational strain (ΔV) is equal to:

$$\Delta V = (1+\varepsilon_1)(1+\varepsilon_2)(1+\varepsilon_3) - 1 = J_1 + J_2 + J_3$$

$J_1,\ J_2,\ J_3$ – are invariants of the strain tensor. Under large strains, the assumption that the conventional dilatational strain can be expressed only by the first invariant of the strain tensor, i.e.
$\Delta V \cong \varepsilon_1 + \varepsilon_2 + \varepsilon_3 = J_1$, – is a kind of approximation, and thus does not present precisely the dilatational strain. Bearing in mind the above–mentioned assumptions, the value of the tensile force on the basis of (10) is equal to:

$$F = \sigma(\varepsilon) A_0 e^{-\varepsilon_{t1}}$$

or, if:

$$e^{\varepsilon_{t1}} = 1 + \varepsilon_1$$

and:

$$\varepsilon_1 = e^{\varepsilon_{t1}} - 1$$

then:

$$F = \sigma(\varepsilon) \frac{A_0}{1+\varepsilon_1} \tag{12}$$

Assuming in the calculations the relationship $\sigma(\varepsilon)$ according to formula (3) for the rectangular cross–section $A_0 = b_0 h_0$, we obtain the value of the force as a function of strains:

$$F = \sigma_o \left(\frac{\varepsilon}{\varepsilon_o}\right)^p \frac{b_0 h_0}{1+\varepsilon} \tag{13}$$

Stress according to conventional strains σ_{eng}(MPa) "engineering stress" has been shown in Fig. 10.

Stress as a function of logarithmic strains σ_{real}(MPa) $\sigma_{eng}(\varepsilon) = \sigma_o \left(\frac{\varepsilon}{\varepsilon_o}\right)^p$

Tension diagrams $\sigma(\varepsilon)$ obtained according to formula (14), as a function of logarithmic strains according to formula (8) is presented in Fig. 7.

$$\sigma(\varepsilon) = \sigma_{real} = \frac{F\,(1+\varepsilon)}{A_0} \qquad \sigma_{real}(\varepsilon) = \sigma_{eng}(\varepsilon)\,(1+\varepsilon) \tag{14}$$

3. Theoretical description of strains in bi–polar coordinates - generalisation of the Bridgman solution

The analysis of the state of strain and stress in necking has been described in [1, 4] and al. However, the state of stress has been generally analysed in necking and a description of strains has been presented in cylindrical coordinates. In the present study, the state of strain and stress has been described in the whole specimen (neglecting the gripped parts only) with bi-polar coordinates (these coordinates have been described, among others, in books [3], [9]). The strain distributions corresponding to the phase prior to the specimen fracture in bi-polar coordinates are shown in Fig.7.

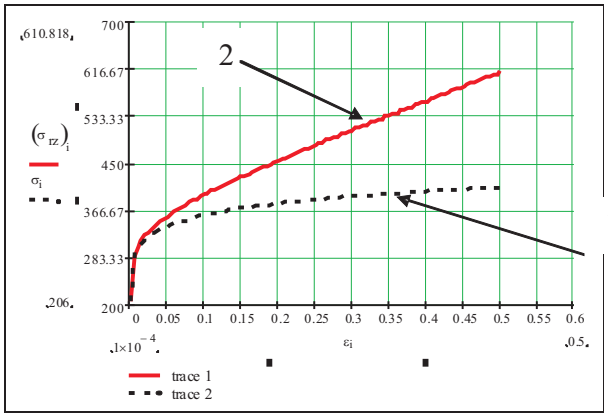

Figure 6 Tension diagrams: $1 - \sigma(\varepsilon)$ according to conventional strains σ_{eng} according to formula (5), 2 – according to (14) as a function of logarithmic strains

The lines showing main strains obtained experimentally can be described approximately in bi–polar coordinates by dividing the specimen into two basic elements: necking in the place of rupture and the "gripped" part that is subject to smaller plastic strains (Fig. 8). The location of necking has been described by means of the variables: ζ, α, β.

$$\zeta = \alpha + i\beta \quad \text{and} \quad \zeta = \ln\frac{a+z}{a-z} \quad \text{where: } z = x + iy$$

$$x = \frac{a\sinh(\alpha)}{\cosh(\alpha)+\cos(\beta)} \qquad y = \frac{a\sin(\beta)}{\cosh(\alpha)+\cos(\beta)} \tag{15}$$

$$\alpha = \ln\frac{\sqrt{(x+a)^2+y^2}}{\sqrt{(x-a)^2+y^2}} \qquad \beta = \arctan\frac{y}{a+x} - \arctan\frac{y}{a-x}$$

$$\rho_1 = \frac{a_1}{|sh\alpha_o|} \qquad R_1 = \frac{a_1}{|\sin\beta_o|} \qquad d_1 = a_1\,|\coth\alpha_o| \qquad r_1 = a_1\left|\tanh\frac{\alpha_o}{2}\right|$$

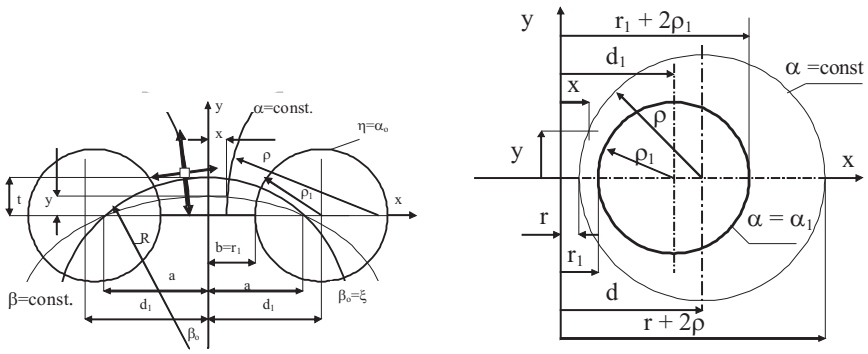

Figure 7 Bi–polar coordinates assumed in the calculations

Strains in the part subject to smaller plastic strains have been also presented in the bi–polar coordinates η, R_2 and ξ, ρ_2. For the "gripped" part, strains have been described through a transformation of the coordinate system (rotation by 90 ° and translation by L) with an exchange of variables. The lines $\alpha = const$ transform into the lines ξ, the lines $\beta = const$ transform into the lines $\eta = const$ ($\zeta_2 = \xi + i\eta$).

$$
\begin{aligned}
x_2 &= \frac{a_2 \sin(\eta)}{\cosh(\xi) + \cos(\eta)} \qquad y_2 = l_1 - \frac{a_2 \sinh(\xi)}{\cosh(\xi) + \cos(\eta)} \\
l_1 &= \frac{a_1 \sin\beta}{\cosh\alpha + \cos\beta} + \frac{a_2 \sinh\xi}{\cosh\xi + \cos\eta} \qquad \rho_2 = \frac{a_2}{|sh\xi|} \\
R_2 &= \frac{a_2}{|\sin\eta|} \qquad b_0 = 2a_2 \left| tg\frac{\eta_o}{2} \right|
\end{aligned}
\tag{16}
$$

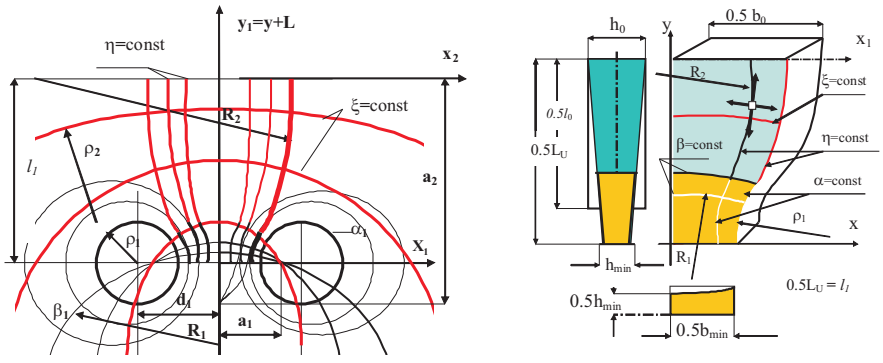

Figure 8 Bi–polar coordinates – division into two basic elements: necking and the rupture point, and the "gripped" part

The solution to the problem in cylindrical coordinates is presented in, for instance, [1, 4]. In these references, an approximate integration of the equations of equilibrium for specimens with the circular cross–section has been performed. In the case of flat specimens, an analogous method can be used. The description of strains in bi–polar coordinates enables a division into two basic elements: necking (point of rupture) and a part that is subject to smaller plastic strains.

3.1. *Calculations of strains*

The strains corresponding to necking, obtained on the basis of the experimental data, can be described in bi–polar coordinates. The specimen length subject to necking – $L_{U2} = 2l_1$, the radii of main curvatures ρ_2 and R_2, the specimen width b_1 are equal to, respectively:

$$\begin{aligned} l_1 &= \frac{a_1 \sin\beta}{\cosh\alpha + \cos\beta} + \frac{a_2 \sinh\xi}{\cosh\xi + \cos\eta} \qquad \rho_2 = \frac{a_2}{|sh\xi|} \\ R_2 &= \frac{a_2}{|\sin\eta|} \qquad b_1 = a_2 \left| tg\frac{\eta_o}{2} \right| \end{aligned} \tag{17}$$

In the upper part, the variables ξ, η have to satisfy the conditions $0 \le \eta \le \eta_0$, – $\xi_0 \le \xi \le 0$. On the other hand, it has been assumed that the dimensions of the cross–section vary according to relationship (4) where: $\Delta\varepsilon = \varepsilon_{\max} - \varepsilon_{kr}$ and the length l_1 is equal to half the length of L_{U2}, hence $l_1 = 0.5L_{U2}$,

$$L_{U2} = L_{01}(1 + \varepsilon_{kr})\,(1 + \Delta\varepsilon)$$

Taking into account relationships (16) and (17) and the conditions of continuity along the joint of the lower and upper part, we obtain a system of equations that allows us to describe strains in bi–polar coordinates:

$$\begin{aligned} & b_0\,(1 - \nu_{pl}\varepsilon_{kr}) = 2a_2 \left| tg\frac{\eta_o}{2} \right| \\ & b_0\,(1 - \nu_{pl} \cdot \varepsilon_{kr})\,(1 - 2\nu_{pl}\Delta\varepsilon) = 2ta_1 \left| tgh\frac{\alpha_o}{2} \right| \\ & l_1 = \frac{a_1 \sin(\beta_0)}{1 + \cos(\beta_0)} + \frac{a_2 \sinh(\xi_0)}{\cosh(\xi_0) + 1} \\ & \frac{a_1 \sinh(\alpha_0)}{\cosh(\alpha_0) + \cos(\beta_0)} = \frac{a_2 \sin(\eta_0)}{\cosh(\xi_0) + \cos(\eta_0)} \\ & \frac{a_1}{|\sin\beta_o|} = \frac{a_2}{|sh\xi_0|} \qquad l_1 = \frac{a_1 \sin(\beta_0)}{\cosh(\alpha_0) + \cos(\beta_0)} + \frac{a_2 \sinh(\xi_0)}{\cosh(\xi_0) + \cos(\eta_0)} \end{aligned} \tag{18}$$

Additionally, it is known that:

$$\sin^2\beta_0 + \cos^2\beta_0 = 1 \qquad \cosh^2\alpha_0 - \sinh^2\alpha_0 = 1$$

$$\sin^2\eta_0 + \cos^2\eta_0 = 1 \qquad \cosh^2\xi_0 - \sinh^2\xi_0 = 1$$

An example: the data for calculations are assumed on the basis of the experimental investigations. The initial dimensions are as follows: $b_0 = 60.0$ mm, $l_0 = 140$ mm,

$h_0 = 1.86$ mm, $l_1 = 93.147$ mm, the coefficient of deformation ν_{pl}, corresponding to the Poisson's ratio, has been calculated according to (6), the values of strains corresponding to the maximum tensile force ε_{kr} and the force corresponding to rupture ε_{max} are equal to $\varepsilon_{kr} = 0.2$, $\varepsilon_{max} = 0.375$ ($\varepsilon_{max} = 0.44$), respectively. The dimensions of the specimen after it has been subjected to strain and necking are as follows: $b_1 = 54.06$ mm, $b_2 = 47.64$ mm, $b_{min} = 40.08$ mm $\rightarrow b_1 = b_0(1 - 2\nu_{pl}\Delta\varepsilon_k)$. Distribution of strains in the failure are shown in Fig. 9. Having solved system of equations (18), we obtain the parameters that describe changes in the specimen dimensions corresponding to necking in bi–polar coordinates:
$a_1 = 112.18$ mm, $\rho_1 = 304.09$ mm, $\alpha_0 = 0.361$, $\beta_0 = 0.795$, $R_1 = 157.14$ mm and $a_2 = 128.76$ mm, $\rho_2 = 157.1$ mm, $\eta_0 = 0.414$, $R_2 = 280.8$ mm, $\xi_0 =$ - 0.748.

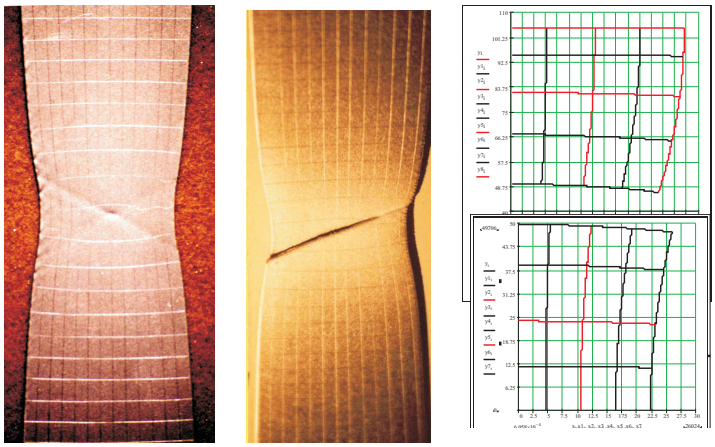

Figure 9 Distribution of strains in the failure phase for St3s and St4s steel and the strain lines in bi–polar coordinates, with a division into two basic elements: the point of rupture and the gripped part

Employing the equations of equilibrium for the Cartesian system of coordinates (x, y), assumed for the whole specimen, the state of strain in the phase prior to rupture can be described:

$$\frac{\partial \sigma_x}{\partial x} + \frac{\partial \tau_{xy}}{\partial y} = 0 \qquad \frac{\partial \tau_{xy}}{\partial x} + \frac{\partial \sigma_y}{\partial y} = 0$$

Assuming that the relationships between main strain lines in the phase of plastic yield can be described in approximation by the proportions (Fig. 7):

$$\frac{r_1}{x} = \frac{x + 2\rho}{r_1 + 2\rho_1} \quad \Rightarrow \quad \frac{1}{\rho} = \frac{2x}{r_1^2 + 2\rho_1 r_1 - x^2} \tag{19}$$

Next, assuming that:

$$\tau_{xy} = \frac{\sigma_y - \sigma_x}{2} \sin 2\varphi \equiv \sigma_{int}\varphi \quad \text{for } \varphi \rightarrow 0 \quad \sin 2\varphi \cong 2\varphi \quad \varphi \cong \frac{y}{\rho} \tag{20}$$

for $y = 0 \quad \sigma_y - \sigma_x = \sigma_{int}$ on the basis of the first equation of equilibrium:

$$\frac{\partial \tau_{xy}}{\partial y} = \sigma_{int} \frac{\partial \varphi}{\partial y}$$
$$\frac{\partial \sigma_x}{\partial x} = -\sigma_{int} \frac{2x}{r_1^2 + 2\rho_1 r_1 - x^2} \Rightarrow \sigma_x = \sigma_{int} \ln\left(r_1^2 + 2\rho_1 r_1 - x^2\right) + C$$

The constant C can be calculated from the condition for $x = r_1 \quad \sigma_x = 0$, then for $y \to 0$

$$\sigma_x = \sigma_{int} \ln \frac{r_1^2 + 2\rho_1 r_1 - x^2}{2\rho_1 r_1} \qquad \sigma_y = \sigma_{int} \left(1 + \ln \frac{r_1^2 + 2\rho_1 r_1 - x^2}{2\rho_1 r_1}\right) \tag{21}$$

whereas, for $y \neq 0$, one should check if the second equation of equilibrium and boundary conditions are fulfilled.

Assuming that

$$\tau_{xy} \equiv \sigma_{int} \varphi = \sigma_{int} \cdot \frac{2xy}{r_1^2 + 2\rho_1 r_1 - x^2}$$

on the basis of the second equation of equilibrium, we obtain:

$$\sigma_y = -\sigma_{int} \left(\frac{y^2}{r_1^2 + 2\rho_1 r_1 - x^2} + \frac{2x^2 y^2}{(r_1^2 + 2\rho_1 r_1 - x^2)^2}\right) + C_2$$

hence, the constant C_2 can be calculated if we know the stress σ_y for $y = 0$ according to formula (21), and thus:

$$\sigma_y = \sigma_{int} \left(1 + \ln \frac{r_1^2 + 2\rho_1 r_1 - x^2}{2\rho_1 r_1} - \frac{y^2 \left(r_1^2 + 2\rho_1 r_1 + x^2\right)}{(r_1^2 + 2\rho_1 r_1 - x^2)^2}\right) \tag{22}$$

The above-mentioned solution describes the components of stresses in Cartesian coordinates. However, taking into consideration changes in curvatures of main strains, it is easier to describe the components of stresses in the part subject to necking in curvilinear coordinates.

3.2. *Analysis of stresses in bi-polar coordinates*

On the basis of physical and geometrical relations for plane stress for flat specimens, strains and stresses can be calculated on the basis of the Lamé equations, then the following equations hold in necking:

$$\frac{\partial \sigma_\beta}{\partial s_\alpha} + \frac{\sigma_\beta - \sigma_\alpha}{R_1} = 0 \qquad \frac{\partial \sigma_\alpha}{\partial s_\beta} + \frac{\sigma_\beta - \sigma_\alpha}{\rho_1} = 0 \tag{23}$$

Assuming that $\sigma_{int} = \sigma_\beta - \sigma_\alpha$, we obtain:

$$\sigma_\alpha = \sigma_{int} \ln \frac{\cosh \alpha_o + \cos \beta}{\cosh \alpha + \cos \beta}$$
$$\sigma_\beta = \sigma_{int} \left[1 + \ln \frac{(\cosh \alpha_o + 1)(\cosh \alpha + \cos \beta)}{(\cosh \alpha + 1)^2}\right] \tag{24}$$
$$\sigma_z = 0 \qquad \varepsilon_z = -\left(\frac{\sigma_{int}}{\sigma_o}\right)^{n-1} \frac{\varepsilon_o}{2\sigma_o} (\sigma_\alpha + \sigma_\beta)$$

The specimen thickness $h(\alpha,\ \beta)$ can be calculated in approximation according to:

$$h(\alpha,\beta) = h_0(1+\varepsilon_z) = h_0\left[1-\left(\frac{\sigma_{int}}{\sigma_o}\right)^{n-1}\frac{\varepsilon_o}{2\sigma_o}\left(\sigma_\alpha+\sigma_\beta\right)\right] \tag{25}$$

Under the assumption of plane stress on the specimen surface, the intensities of stresses and strains are equal to, respectively:

$$\sigma_{int} = \sqrt{\sigma_\alpha^2 - \sigma_\alpha\sigma_\beta + \sigma_\beta^2}, \quad \varepsilon_{int} = \varepsilon_0\left(\frac{\sigma_{int}}{\sigma_0}\right)^n \tag{26}$$

where σ_{int} is the stress intensity according to the Huber – Mises hypothesis. On the basis of the boundary conditions along the line that connects the upper and lower part: for $\beta = \pi/2$ and $\xi = -\pi/2 \quad \sigma_\beta = \sigma_\xi$ and $\sigma_\alpha = \sigma_\eta$ for $\eta = 0.492 \quad \sigma_\eta = 0$, for $y = L \quad \sigma_y = \sigma_o$, and then we obtain the stress components.

In the "gripped" part, the Lamé equations have the form:

$$\begin{aligned}
&\frac{\partial\sigma_\xi}{\partial s_\eta} + \frac{\sigma_\xi - \sigma_\eta}{\rho_2} = 0 \qquad \frac{\partial\sigma_\eta}{\partial s_\xi} + \frac{\sigma_\xi - \sigma_\eta}{R_2} = 0\\
&\sigma_{\eta i} = -\sigma_{0i}\ln\frac{\cosh\xi_i + \cos\eta_0}{\cosh\xi_i + \cos\eta_i}\\
&\sigma_{\xi i} = \sigma_{oi}\left[1 - \ln\frac{\left(1+\cos\eta_0\right)\left(\cosh\xi_i + \cos\eta_i\right)}{\left(1+\cos\eta_i\right)^2}\right]
\end{aligned} \tag{27}$$

where σ_{0i} is the stress acting along the line connecting the upper and lower part, calculated on the basis of the conditions of continuity along the line $\beta_o = \xi_o = const.$

$$\begin{aligned}
\sigma_{0i} \quad = \quad & \sigma_{int}\left[1 + \ln\frac{\left(\cosh\alpha_0 + 1\right)\left(\cosh\alpha_i + \cos\beta_0\right)}{\left(\cosh\alpha_i + 1\right)^2}\right]\\
& \left[1 - \ln\frac{\left(1+\cos\eta_0\right)\cdot\left(\cosh\xi_i + \cos\eta_0\right)}{\left(1+\cos\eta_i\right)^2}\right]^{-1}
\end{aligned}$$

A mean value of the stress intensity σ_{int} can be calculated if the dimensions of the specimen in its cross–section subject to necking are known. Having divided the force causing necking by the cross–section corresponding to it for $\beta = 0$, we obtain the integral equation, on the basis of which we calculate σ_{int}:

$$\sigma_{int} = \frac{F}{2\int\limits_0^{\alpha_0} h(\alpha,\ \beta)\cos\varphi ds_\beta} \tag{28}$$

where F is calculated from formula (13), and $h(\alpha,\ \beta)$ – from formula (25). An example of calculations of the stress (σ_{int}) is shown in Fig. 10.

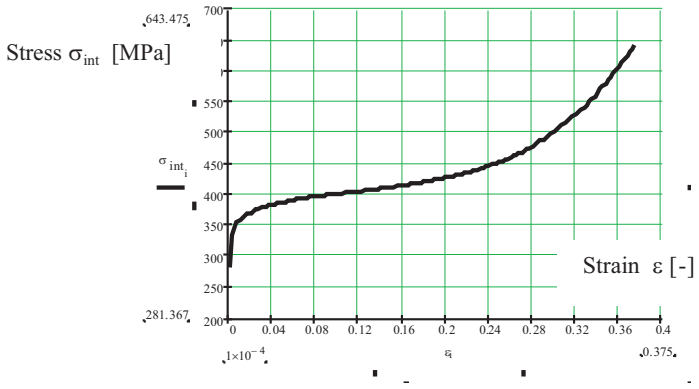

Figure 10 Tension diagrams $\sigma(\varepsilon)$ obtained according to formula (28), after taking into account strain hardening and necking

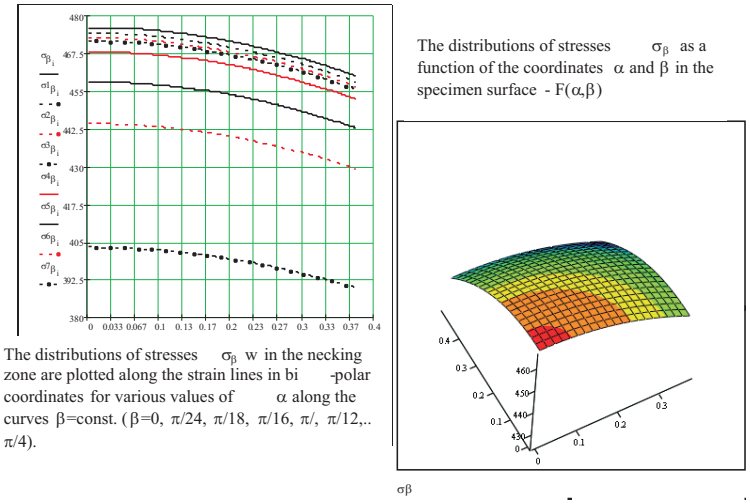

Figure 11 Distributions of the normal stresses σ_β according to formula (24) in the necking zone

3.3. *Results of analytical calculations of stresses and strains in the phase prior to rupture*

The analysis of strains and stresses made by means of analytical and numerical methods was based on tensile tests in the phase of failure. The results of analytical numerical calculations obtained with the "MATHCAD 2001" software package and the FEM code (ANSYS 12 and 14) are presented below. The distributions of stresses σ_β and σ_α calculated on the basis of equations (24) and the intensities of stresses and strains in the necking region (as a function of the coordinates α and β) according to (16) are depicted in Figs. 13÷18.

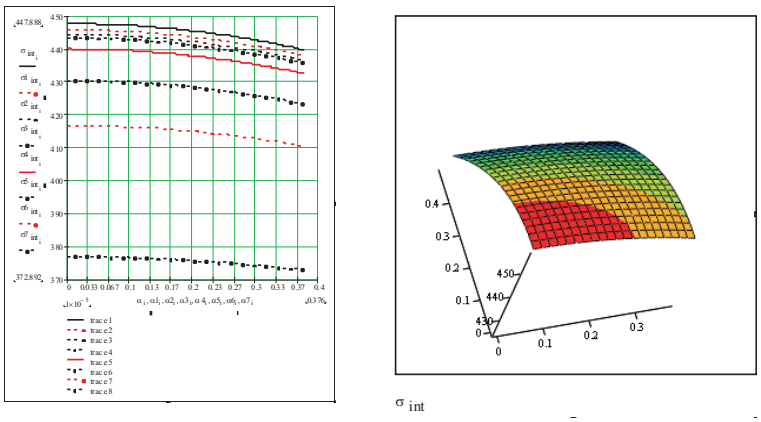

Figure 12 Distribution of the reduced stresses σ_{int} (stress intensity) according to the Huber hypothesis, according to formula (26)

The curves showing a variability of the stresses σ_β and σ_α and changes in the stress and strain intensities σ_{int} and ε_{int}, respectively, in the necking zone are plotted along the strain lines in bi–polar coordinates (Fig. 8) for various values of α along the curves $\beta = const$ ($\beta = 0$, $\pi/24$, $\pi/18$, $\pi/16$, $\pi/12$, ... $\pi/4$) and in the form of surface functions $F(a_1, \alpha, \beta)$ (for two variables α and β). The changes in the specimen thickness calculated according to (25) were compared to the test results obtained with the moiré–fringe technique.

The distributions of strains prior to an occurrence of the central fissure (in the middle of the specimen) and strains on the specimen surface obtained with the moiré–fringe technique were compared to the calculation results. The differences in the measured and calculated changes in the specimen thickness Δh were equal to 2÷6 %.

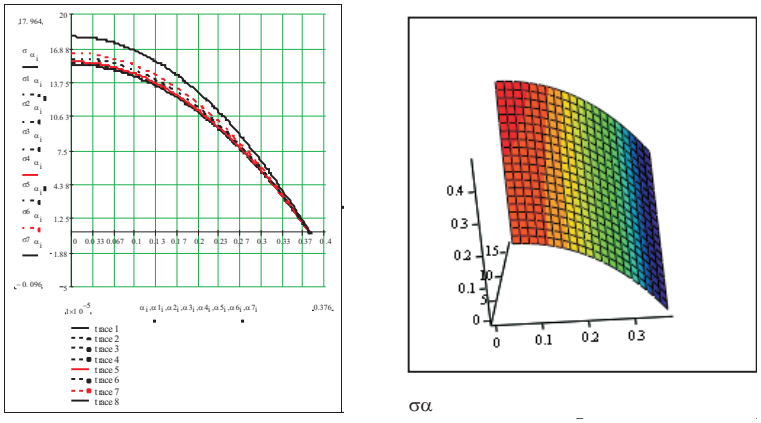

Figure 13 Distributions of the normal stresses σ_α according to formula (24) in the necking zone

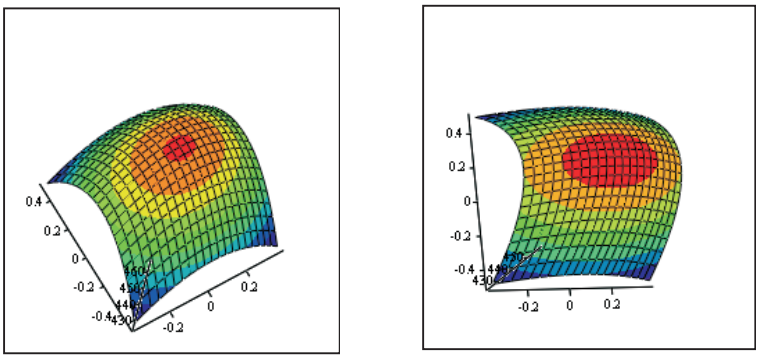

Figure 14 Distributions of the normal stresses σ_β and the reduced stresses -σ_{int} (stress intensity) according to the Huber hypothesis in the necking zone

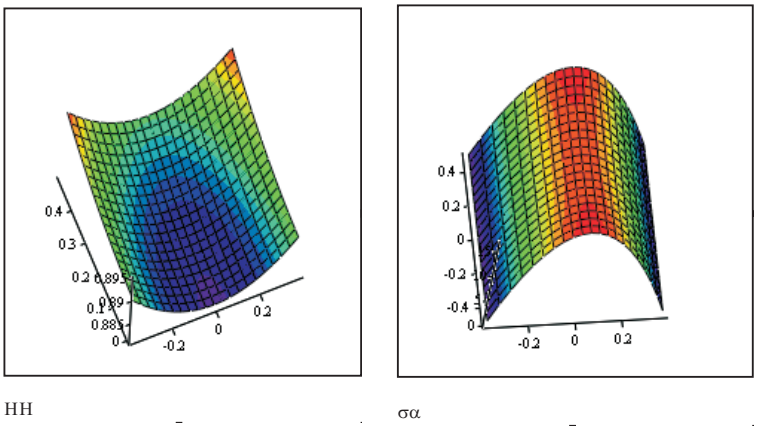

Figure 15 Changes in the specimen thickness Δh from the axis of symmetry. Distributions of the normal stresses σ_α in the necking zone

3.4. *Zones of sliding lines (surfaces)*

Under further loading, plastic strain zones and sliding lines (surfaces) start to occur and they can be described as a function of two variables $x(\alpha, \beta)$, $y(\alpha, \beta)$ on the basis of well–known relationships:

$$\frac{dy}{dx} = \pm\frac{2\left(\tau_{xy} - k\right)}{\sigma_y - \sigma_x} \quad \text{or:} \quad \frac{dy}{dx} = \pm\frac{\sigma_y - \sigma_x}{2\left(\tau_{xy} - k\right)} \quad \text{where: } k = \frac{\sigma_{int}}{\sqrt{3}} \tag{29}$$

The zones of plastic strains and sliding lines (surfaces) can be described on the basis of the main strain lines x(α, β), $y(\alpha, \beta)$, whereas the stress components have been calculated according to formulas (24) and (26)

1. Assuming that:

$$\sigma_{int} = \sigma_\beta - \sigma_\alpha \qquad \tau_{xy} = \frac{\sigma_\beta - \sigma_\alpha}{2} \sin 2\varphi \quad \text{and } \sigma_y - \sigma_x = (\sigma_\beta - \sigma_\alpha) \cos 2\varphi$$

we obtain:

$$\frac{dy}{dx} = \pm \frac{\sigma_{int} \sin 2\varphi - 2k}{\sigma_{int} \cos 2\varphi} \quad \Rightarrow \quad \frac{dy}{dx} = \pm \left(tg2\varphi - \frac{2k}{\sigma_{int} \cos 2\varphi} \right) \tag{30}$$

After the integration:

$$y = \pm x \left(tg2\varphi - \frac{2k}{\sigma_{int} \cos 2\varphi} \right) + C_2 \tag{31}$$

where:

$$\sin 2\varphi = \frac{2sh\alpha_i \sin \beta_i \left[(1 + ch\alpha_i) \cos \beta_i \right]}{(ch\alpha_i + \cos \beta_i)^2} \qquad \cos 2\varphi = \frac{2 - (ch\alpha_i - \cos \beta_i)^2}{(ch\alpha_i + \cos \beta_i)^2}$$

2. Assuming that plain stress occurs on the specimen surface, the intensity of stresses and strains have been calculated according to formula (26), and the sliding surface shape according to the following formula:

$$\frac{dy}{dx} = \pm \frac{\sigma_{int} \cos 2\varphi}{\sigma_{int} \sin 2\varphi - 2k} \qquad y = \pm\, x \left(\frac{\sigma_{int} \cos 2\varphi}{\sigma_{int} \sin 2\varphi - 2k} \right) + C_2 \tag{32}$$

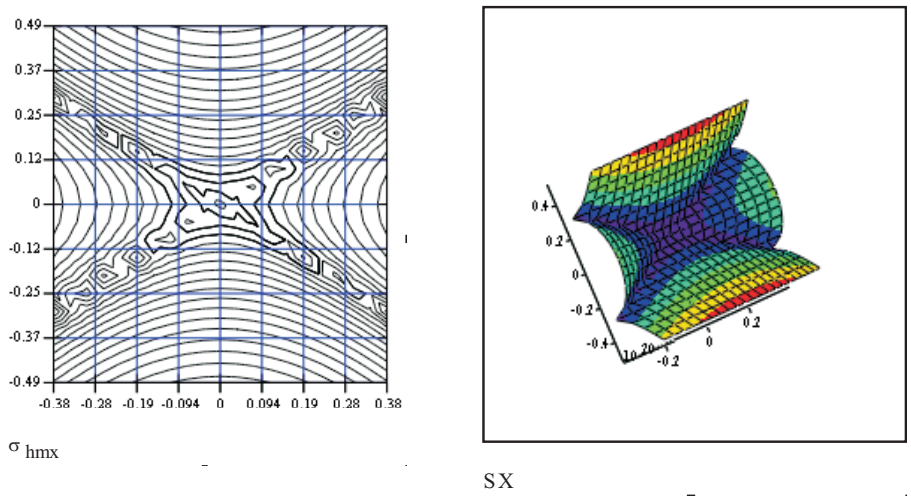

Figure 16 Zones of the plastic strains and the sliding lines (surfaces) at the point of necking prior to fracture, calculated according to (26)

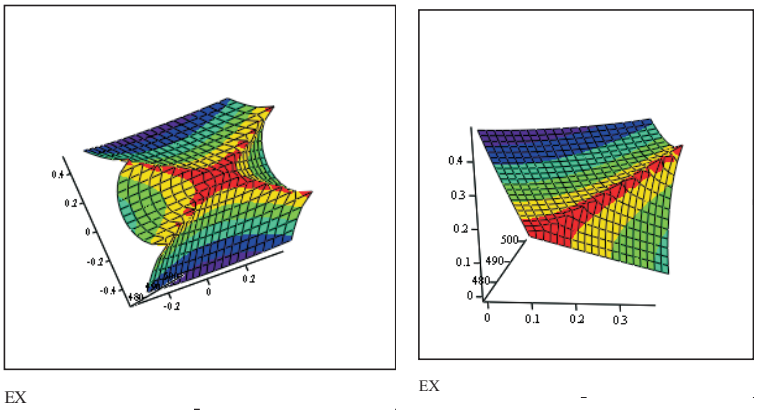

Figure 17 Distributions of the reduced stresses according to the Huber hypothesis along the sliding line at the point of necking prior to fracture, calculated according to (30)

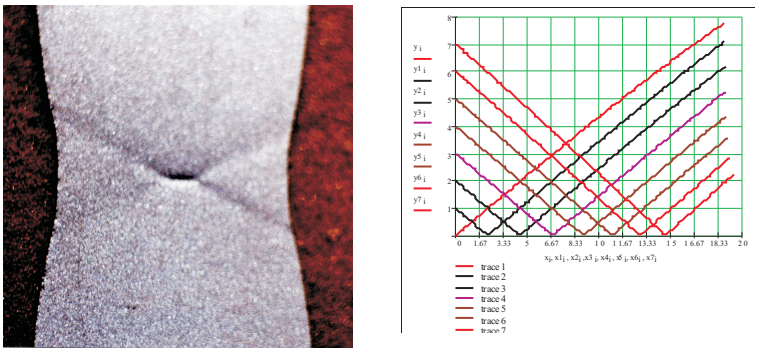

Figure 18 Specimen surface in strain and the sliding lines, calculated according to (32). Due to the two–axis symmetry, 1/4 of the specimen has been presented at the point of necking

3.5. *Results of numerical calculations of the specimen under test*

The results of experimental investigations and calculations have been compared to the results of numerical calculations (with the finite element method, using the ANSYS 6.1 software package). In the model for numerical calculations, the dimensions such as in the initial phase of necking have been assumed. (Fig. 3). The material properties $\sigma(\varepsilon)$ assumed in the computations in the form of a polygonal curve correspond to actual stresses and strains at the point of necking (Fig. 19).

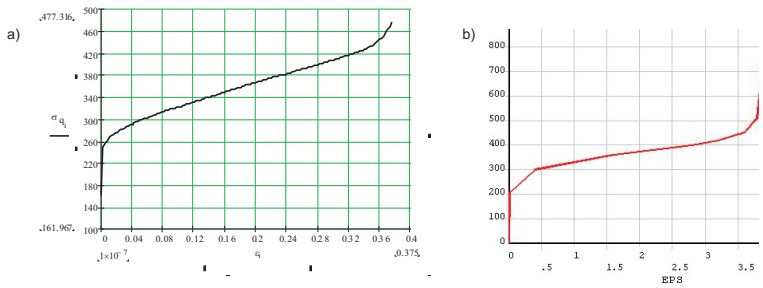

Figure 19 Material properties $\sigma(\varepsilon)$: a) obtained from the tests, b) assumed in the FEM computations

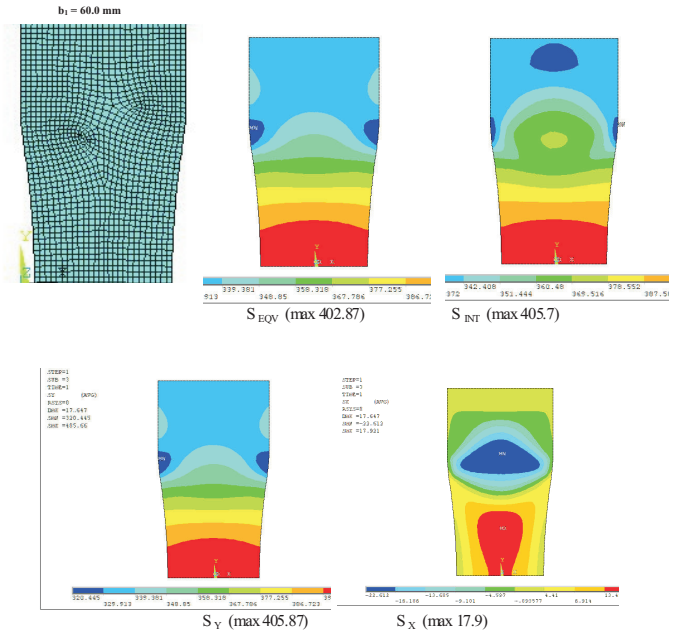

Figure 20 Results obtained on the basis of the FEM numerical calculations (ANSYS 12). The drawings show: a mesh of elements, distributions of the reduced stresses according to the Huber hypothesis and distributions of the maximum shear stresses τ_{max}, distributions of the normal stresses σ_y and σ_x

4. Conclusions following from the tensile test

The conducted tests and numerical calculations of the tensile test are aimed at the verification of the mathematical model that can be applied in further computations. The presented formulae enable a description of stresses in the whole range of loading, taking into account necking and a determination of the intensity of stresses, a

description of the generation of the sliding lines, or strictly speaking, the sliding surfaces.

The way the strains have been described in bi–polar coordinates, which has been based on experimental investigations, allows for employing the results into numerical calculations, where we are interested in stress states in failure. The description of the stress–strain relationship, which takes into consideration a strain hardening and necking under rupture and the determination of the magnitude of breaking stresses, makes it possible to develop a numerical model until the element failure occurs. The distributions of strains calculated according to the presented formulae are convergent with the results of strain tests in the neighbourhood of necking.

The simplified analysis of the stress state in bi–polar coordinates can be used to build a numerical model if we assume a division of the specimen into two basic elements: a part that is subjected to uniform tension and a part that has been subjected to uniform tension and then necking.

The scheme of failure can be described as follows: the value of the maximum force obtained during the tensile test and the strain corresponding to it enables a determination of the parameter or the function of strain hardening. In order to obtain the maximum force, we can assume uniform tension, then the necked part is subject to strain as a matter of fact.

While analysing the test results, the following should be defined:

1. strains corresponding to the limit of proportionality and to the yield point,
2. strains corresponding to the maximum tensile force,
3. strains corresponding to necking at the instant of rupture and the dimensions of the cross–section.

Next, an influence of necking, at which an increase in stresses and a rupture of the material cohesion forces take place and a fracture (a vertical central fissure propagating symmetrically along the sliding lines) occurs, and then the material breaks along the sliding line, should be considered.

The sliding lines determined experimentally and analytically in the failure phase go at the angle of 60° with respect to the vertical axis, and not at the angle of 45° as has been assumed in numerous theoretical solutions.

A good agreement between the FEM numerical results (ANSYS 12 and 14) and those obtained from the tests has been found. Because of too little a number of tests, one cannot draw too explicit conclusions, nevertheless the presented actual $\sigma - \varepsilon$ (stress–strain) relationship in the whole range of loading makes it possible to employ the mathematical model that can be applied in further material strength calculations.

References

[1] **Bridgman, P. W.**: Studies in large plastic flow and fracture, *McGraw–Hill*, New York, **1952**.

[2] **Brinson, H. F. and Brinson, L. C.**: Polymer Engineering Science and Viscoelasticity, *Springer Science&Busines Media*, New York, **2015**.

[3] **Chakrabarty, J.**: Theory of plasticity, *Elsevier*, Butterworth–Heinemann, **2006**.

[4] **Hill, R.**: The mathematical theory of plasticity, *Oxford: The Clarendon Press*, **1950**.

[5] **Hutchinson, J. W.**: Singular behaviour at the end of a tensile crack in a hardening material, *J. Mech. Phys. Solids*, Vol. 16, 13–31, **1968**.

[6] **Hoffman, O. and Sachs, G.**: Introduction to the Theory of Plasticity for Engineers, *McGraw–Hill Book Company*, **1953**.

[7] **Jones, R. M.**: Deformation Theory of Plasticity, *Bull Ridge Publishing*, Blacksburg, Virginia USA, **2009**.

[8] **Khalil, A. M and Fazio P.**: Moiré–fringe measurement *Experimental Mechanics*, **1973**.

[9] **Khan, A. S. and Huang, S.**: Continuum Theory of Plasticity, *John Wiley&Sons New York*, Chichester, Brisbane, Toronto, **1995**.

[10] **Krzyś, W. and Życzkowski, M.**: Elasticity and Plasticity – Problems and Examples, (in Polish), *PWN*, Warsaw, **1962**.

[11] **Ludwik, P.**: Elemente der technologischen Mechanik, *Springer*, Berlin, **1909**.

[12] **Mróz, Z.**: Non–associated flow laws in plasticity, *Journal de Mecanique*, 2, 1, 21, **1963**.

[13] **Neimitz, A.**: Mechanics of fracture, (in Polish), *PWN*, Warsaw, **1998**.

[14] **Rice, J. R. and Rosengren, G. F**: Plane Strain Deformation Near a Crack Tip in a Power–Law Hardening Material, *Jurn. Mech. Phys. Solids*, 16, **1968**.

[15] **Rowlands, R. E., Vallem, H.**: On replication for moiré-fringe multiplication, *Experimental Mechanics*, **1980**.

[16] **Sih, G. C.**: Hanbook of Stress–Intensity Factors, *Leigh University Press*, Bethlehem, 1, **1973**.

[17] **Seweryn, A.**: Modelling of singular stress fields using finite element method, *International Journal of Solids and Structures*, 39, 4787–4804, **2002**.

[18] **Shih, C. F. and Hutchinson, J.: W.**: Fully Plastic Solutions and Large Scale Yielding Estimates for Plane Stress Crack Problems, *Journ. of Engineering Materials and Technology*, 76, **1976**.

[19] **Tada, H., Paris, P. and Irwin, G. R.**: The stress analysis of cracks: Handbook, *Hellertown: Del Research Corp.*, 385 **1973**.

[20] **Timoschenko, S.**: Theory of Elasticity, *John Wiley*, New York, **1980**.

[21] **Tvergaard, V. and Hutchinson, J. W.**: Effect of strain–dependent cohesive zone model on prediction of crack growth resistance, *Int. J. Solid Structures*, 33, 3297–3308, **1996**.

[22] **User's Guide ANSYS**, 12, 14, *Ansys, Inc.*, Huston, USA, **2014**.

[23] **Wegner, T.**: Surface of limit state in nonlinear material and its relation with plasticity condition, *The Archive of Mechanical Engineering*, XLVII, 3, 205–223, **2000**.

[24] **Wegner, T.**: A method of material modelling with the use of strength hypothesis of inner equilibrium stability, *Mechanics and Mechanical Engineering*, 4, 2, p. 139–147, **2000**.

[25] **Zienkiewicz, O. C.**: The Finite Element Method in Engineering Science, *McGraw–Hill*, London, New York, **1971**.